B. Corrections and Changes Made

In the following list of changes made, the section numbers and page numbers refer to the original text as quoted in the correction sheet and could have changed in the latest version of the text.

B.1. Mairi's Corrections

B.1.1. Point 1: Short corrections

The changes have been made. In the case of one of the corrections the notation K_1, K_2, K_3 was to be changed to k_1, k_2, k_3. However the K_i as used refer to the range of k values in the simulation and not to individual k_i values so this has not been changed.

B.1.2. Point 2: Drawbacks of Inflation

Added to discussion on Pg 36:

In this thesis inflation is taken to be the mechanism by which inhomogeneities in matter are seeded and the horizon and flatness problems of the Big Bang are solved. However, the inflationary paradigm is not without its own challenges.

Chief amongst these is the lack of a unique underlying theory. Many high energy theories have been shown to produce an inflationary phase. Often, however, these require a great deal of fine-tuning in order to produce a sufficient number of e-foldings of inflation. Lack of knowledge about the governing physics at high energy scales hampers our understanding of the cause of inflation and undermines any analysis of the generic nature of the initial conditions required.

The overall duration of inflation is also unknown. Observations only require that currently observable scales were previously inside the horizon. Thus the onset of inflation is not constrained and could occur far in the past. However, allowing such a long inflationary period typically increases the fine-tuning necessary and can lead to other issues.

There are further problems with the inflationary paradigm, including the lack of an explanation for how energy in the inflaton field is transferred to the other constituent parts of the universe, and indeed the fact that no scalar field has yet been directly observed.

We will continue to employ the inflationary paradigm in this thesis but it is important to acknowledge that some challenges remain to be overcome.

B.1.3. Point 3: T-duality discussion

Inserted on Pg 40 just below Section 3.2.2 header:

In string theory an extra space time symmetry is present which relates physical properties in theories with large compactification radius with those in theories with small radius. Suppose we have a string theory compactified on a circle of radius L. The "T-duality" transformation which relates two physical theories with this one compactified dimension is

$$L \to \widetilde{L} = \frac{\alpha'}{L}\,. \tag{B.1}$$

Now consider what effect this transformation will have on the momentum of a closed string. Instead of being a continuum, the momentum takes discrete values ...

Rephrased end of Section 3.2.2 on Pg 41 as follows:

The formula for the mass spectrum, Eq. (3.2), is invariant when j and w are exchanged given the transformation in Eq. (3.1). Writing the equations of motion in terms of $\widetilde{L}$, having interchanged j and w, gives a new theory which is compactified on a circle of radius $\widetilde{L}$. This is known as the T-dual theory [94, 167]. The two theories are physically identical since T-duality is an exact symmetry of string theory for closed strings. The T-duality applies to all physics in the theory and in particular also affects open string modes. These behave in a different way under T-duality to closed strings as will be described below.

Rephrased part of Section 3.2.3 on Pg 41 as follows:

We introduced T-duality by explaining its effects on closed strings. But what happens to the open strings in a T-dualised theory? Open strings, as their name suggests, have two open ends and consequently cannot have a conserved winding number such as w. Suppose once more that one of the D dimensions is compactified. As $L \to 0$, the non-zero momentum states become infinitely massive, but in contrast to the closed case there is now no continuum of winding states. Thus, the open string

now lives in $D-1$ dimensions similar to the result of standard KK compactification [86]. The endpoints of the open strings then observe Dirichlet boundary conditions, taking fixed values in the compactified direction. There are still closed strings in this theory, however, and these continue to move in the full D dimensions after being T-dualised.

The result is similar if more than one coordinate is made periodic. If $D-p-1$ spatial dimensions are compactified, for some p, then the ends of the open strings can still move freely in the other p spatial dimensions on a $p+1$ dimensional hypersurface. This hypersurface is called a Dirichlet brane or Dp-brane. The closed string modes move in the full D dimensions.

B.1.4. Point 4: Validity of Eq 3.28

Added to end of Pg 48:

In deriving Eq. (3.28) we have assumed that $r/c_{\rm s}P_{,X}$ varies slowly during observable inflation. For the DBI case, $c_{\rm s}P_{,X}=1$ and the change in r can be related to the change in ϵ_H and $c_{\rm s}$ through Eq. (2.87). As we have taken $\epsilon_H, |\eta_H|, |s| \ll 1$ the tensor-scalar ratio will indeed vary slowly over the observable epoch. For more general models where $c_{\rm s}P_{,X} \neq 1$ we have that

$$\frac{\mathrm{d}}{\mathrm{d}\mathcal{N}}\left[\frac{r}{c_{\rm s}P_{,X}}\right] = 16\frac{\epsilon_H}{P_{,X}}\left(2\epsilon_H - 2\eta_H\right) . \tag{B.2}$$

Therefore $r/c_{\rm s}P_{,X}$ varies slowly as long as $P_{,X}$ is not too small, i.e., close to $\mathcal{O}(\epsilon_H^2)$. This will not be the case in the models studied in Chapters 4 and 5.

B.1.5. Point 5: No isocurvature mode considered

Added to Perturbation section on Pg 24:

For single field models no mixing of adiabatic and non-adiabatic modes occurs [203]. Therefore, throughout this thesis we will only consider adiabatic perturbations and ignore any isocurvature mode present.

B.1.6. Point 6: Assumptions leading to $r < 10^{-7}$

Added to Section 4.2 on Pgs 54 and 55:

Before concluding this section, we should explicitly outline all the assumptions that have lead to Eq. (4.13). First, we are considering the relativistic limit where $c_{\rm s} \ll 1$. We are also restricting ourselves to considering the UV scenario where a

brane moves towards the tip of the throat. This ensures that Eq. (4.5) is satisfied. For the Lyth bound to take the form in Eq. (3.28), we have assumed that r varies slowly during the observable period of inflation. This is justified as the change in r can be written in terms of the quasi deSitter parameters ϵ_H, η_H and s and we have assumed their magnitudes are much less than unity.

...

In order to neglect the $f_{\rm NL}^{\rm eq}$ term in Eq. (4.10) we have assumed that $-f_{\rm NL}^{\rm eq} > 5$. As $c_{\rm s}$ has been taken to be small this is expected to be the case. The volume of the Sasaki-Einstein manifold X_5 is taken to be $\mathcal{O}(\pi^3)$ in keeping with the values for known solutions. The WMAP5 normalisation of the scalar perturbation power spectrum has also been used. Finally, in going from Eq. (4.12) to the final numerical figure in Eq. (4.13) the most "optimistic" value, $\Delta\mathcal{N}_* \simeq 1$, has been chosen as this leads to the least restrictive bound on r. As described above a more realistic value of 4 would severely constrain r due to the strong dependence of Eq. (4.12) on $\Delta\mathcal{N}_*$.

B.1.7. Point 7: Discussion of $Y^{p,q}$

Added to Section 4.3 on Pg 57:

Previously only two five-dimensional Sasaki-Einstein metrics were explicitly known, S^5 and $T^{1,1}$ on $S^2 \times S^3$. The $Y^{p,q}$ metrics described in Ref. [70] are a countably infinite number of Sasaki-Einstein metrics on $S^2 \times S^3$. The metrics are parametrised by the two topological numbers p and q, which are coprime when the $Y^{p,q}$ is topologically $S^2 \times S^3$. The volume of one of these manifolds is proportional to $1/p$. Hence by setting $q = 1$ and letting p become large, this volume can be made arbitrarily small [70]. On the other hand, the largest volume occurs for $p = 2$, $q = 1$ giving $\mathrm{Vol}(Y^{2,1}) \simeq 0.29\pi^3$.

B.1.8. Point 8: Rewrite Section 4.4 more clearly

Many changes have been made to Section 4.4 including splitting the later parts into two subsections. The functions f_1, f_2 and f_3 have been renamed f_A etc in order to avoid confusion with Section 5.2. Many equations from previous sections have been repeated in order to improve readability.

Major changes:

Change to introductory section on Pg 58:

In this section, we take a phenomenological approach and consider the following kinetic function which has a more general form than the DBI one but still contains

a square root term:

$$P = -f_A(\varphi)\sqrt{1 - f_B(\varphi)X} - f_C(\varphi)\,, \tag{B.3}$$

where $f_i(\varphi)$ are unspecified functions of the inflaton field. We will assume implicitly that these functions have a suitable form for generating a successful phase of inflation. A direct comparison with Eq. (3.11) indicates that the standard DBI action can be recovered by setting $f_A f_B = 2$. This implies that $c_{\rm s}P_{,X} = 1$ and greatly simplifies the form of Eq. (4.3). Another important property in the DBI case is that the warp factor uniquely determines the kinetic structure of the action, i.e., $h^4 \propto f_A \propto f_B^{-1}$. In view of this, it is interesting to consider whether the gravitational wave constraints could be weakened by relaxing one or both of these conditions.

We can differentiate $P(X, \varphi)$ in Eq. (4.22) to find:

$$P_{,X} = \frac{f_A f_B}{2\sqrt{1 - f_B X}}\,, \tag{B.4}$$

$$P_{,XX} = \frac{f_A f_B}{2}\frac{f_B}{2(1 - f_B X)^{\frac{3}{2}}}\,. \tag{B.5}$$

The sound speed of fluctuations in the inflaton, defined in Eq. (2.81), is then given by

$$c_{\rm s} = \sqrt{1 - f_B X} = \frac{f_A f_B}{2}\frac{1}{P_{,X}}\,, \tag{B.6}$$

and the scalar power spectrum (2.86) by

$$\mathcal{P}_{\mathcal{R}}^2 = \frac{1}{2\pi^2}\frac{H^4}{f_A f_B \dot{\varphi}^2}\,. \tag{B.7}$$

Explanation of generalisation of BM bound on Pg 59 expanded and revised:

The BM bound (4.4) restricts the maximal variation of the scalar field φ in the full throat region for DBI inflation. This is determined by expression (4.2) for generic warped geometries that are asymptotically $AdS_5 \times X_5$ away from the tip of the throat. However, in Section 3.4 the Lyth bound was also defined for general non-canonical actions. For the more general kinetic function (4.22), the BM bound becomes

$$r < \frac{32}{N(\mathcal{N}_{\rm eff})^2} c_{\rm s} P_{,X} = \frac{16}{N(\mathcal{N}_{\rm eff})^2} f_A f_B\,. \tag{B.8}$$

To use this bound we must be able to calculate $\mathcal{N}_{\rm eff}$ over the full range of e-foldings

of inflation. This requires knowledge of the behaviour of f_A and f_B over that range.

A more cautious approach would be to restrict our attention to the observable stage of inflation. Assuming that the variation of $f_A f_B = 2c_{\rm s}P_{,X}$ is negligible during that epoch, we can use Eq. (3.28) which states that

$$\left(\frac{\Delta\varphi}{M_{\rm PL}}\right)_*^2 \simeq \frac{(\Delta\mathcal{N}_*)^2}{8}\left(\frac{r}{c_{\rm s}P_{,X}}\right)_* = \frac{(\Delta\mathcal{N}_*)^2}{4}\left(\frac{r}{f_A f_B}\right)_* . \tag{B.9}$$

In addition, if observable scales leave the horizon while the brane is inside the throat, the change in the field value must satisfy $|\Delta\varphi_*| < \varphi_{UV}$. It follows from Eqs. (4.31) and (4.32), therefore, that

$$r_* < \frac{32}{N(\Delta\mathcal{N}_*)^2}(c_{\rm s}P_{,X})_* = \frac{16}{N(\Delta\mathcal{N}_*)^2}(f_A f_B)_* . \tag{B.10}$$

Condition (4.33) will be referred to as the generalised BM bound. We have been conservative by restricting our discussion to the observable phase of inflation. A stronger condition is obtained by using Eq. (4.31), which is equivalent to substituting $\Delta\mathcal{N}_* \to \mathcal{N}_{\rm eff}$. If $f_A f_B$ remains nearly constant over the last $\mathcal{N}$ e-foldings of inflation, then $\mathcal{N}_{\rm eff}$ may be as large as 60 and the right hand side of Eq. (4.33) will be reduced by a factor of 225. Thus, the generalised bound (4.33) should be regarded as a necessary (but not sufficient) condition to be satisfied by the tensor modes.

B.1.9. Point 9: Naturalness of multi-coincident brane inflation

Added to Section 5.1 on Pg 65:

One scenario in which multiple branes are expected is after brane flux annihilation, in which branes travelling down the throat annihilate with the trapped flux, creating new branes [53, 90, 194]. These are then attracted by other branes and fluxes in other throats and propagate toward the bulk. In Ref. [194] Thomas & Ward argue that it is unlikely that only a single brane is left after the flux annihilation process, due to the large amount of fine tuning necessary to achieve this. Instead it is more likely that a number of branes remain.

B.1.10. Point 10: Rephrasing of Section 5.4 about large n limit

Two subsection headers have been inserted and the main bulk of Section 5.4 has been rephrased. A factor of 2 error has been fixed but conclusions remain the same.

Reworked section:

The regime $W \gg 1$ is of interest for relaxing the gravitational wave constraints[1]. The generalised BM bound for IR models, with branes propagating towards the bulk, is given by Eq. (4.37):

$$\frac{f_2 M_{\rm PL}^4}{N} > \frac{(\Delta\mathcal{N}_*)^2}{4\pi^2}\frac{\sqrt{-3f_{\rm NL}^{\rm eq}}}{(1-n_s)\mathcal{P}_{\mathcal{R}}^2}\,. \tag{B.11}$$

As we know f_2, this may be expressed as a limit on the value of the warp factor $h(\varphi_*)$ on CMB scales:

$$NT_3\left(\frac{h_*}{M_{\rm PL}}\right)^4 < \frac{8\pi^2(1-n_s)\mathcal{P}_{\mathcal{R}}^2}{\sqrt{-3f_{\rm NL}^{\rm eq}}(\Delta\mathcal{N}_*)^2}\,. \tag{B.12}$$

We now consider whether this limit can be satisfied for reasonable choices of parameters when the warped compactification corresponds to an AdS_5 or KS throat, respectively. Recall that the warp factor for the AdS_5 throat is given by $h = \varphi/(\sqrt{T_3}L)$. Condition (5.28) therefore reduces to a constraint on the value of the inflaton during observable inflation:

$$\frac{\varphi_*^4}{M_{\rm PL}^4} < \frac{8\pi^2(1-n_s)\mathcal{P}_{\mathcal{R}}^2}{\sqrt{-3f_{\rm NL}^{\rm eq}}(\Delta\mathcal{N}_*)^2}\frac{T_3L^4}{N}\,. \tag{B.13}$$

However, non-perturbative string effects are expected to become important below a cutoff scale, $\varphi_{\rm cut} = h_{\rm cut}\sqrt{T_3}L$, where $h_{\rm cut}$ is the value of the warp factor at that scale. For consistency, therefore, one requires $\varphi_* > \varphi_{\rm cut}$, so that

$$NT_3\left(\frac{h_{\rm cut}}{M_{\rm PL}}\right)^4 < \frac{8\pi^2(1-n_s)\mathcal{P}_{\mathcal{R}}^2}{\sqrt{-3f_{\rm NL}^{\rm eq}}(\Delta\mathcal{N}_*)^2}\,, \tag{B.14}$$

[1]Note that the case $n \gg 1$ and $W \sim 1$ will not significantly relax the BM bound, since we require $n \ll N$ for backreaction effects to be negligible.

which implies an upper limit on the D3-brane charge:

$$N < \frac{64\pi^5 g_{\rm s}(1-n_s)\mathcal{P}_{\mathcal{R}}^2}{\sqrt{-3f_{\rm NL}^{\rm eq}}(\Delta\mathcal{N}_*)^2}\left(\frac{M_{\rm PL}}{h_{\rm cut}m_{\rm s}}\right)^4 . \tag{B.15}$$

Assuming the typical values $m_{\rm s} \sim 10^{-2}M_{\rm PL}$, $\Delta\mathcal{N}_* \simeq 4$ and $h_{\rm cut} \sim 10^{-2}$ implies

$$N < 1.76 \times 10^8 (1-n_s)(-f_{\rm NL}^{\rm eq})^{-1/2} , \tag{B.16}$$

and for $1 - n_s < 0.05$ and $-f_{\rm NL}^{\rm eq} > 5$ the inequality becomes

$$N < 4 \times 10^6 . \tag{B.17}$$

For an AdS_5 throat, the fuzzy potential W is a constant, and the condition that $W \gg 1$ becomes

$$\hat{C} \ll \frac{4\pi^2 g_{\rm s} N}{{\rm Vol}(X_5)} . \tag{B.18}$$

Hence, combining inequalities (5.31) and (5.34) implies that

$$\hat{C} \ll \frac{2(2\pi)^7(1-n_s)\mathcal{P}_{\mathcal{R}}^2}{\sqrt{-3f_{\rm NL}^{\rm eq}}(\Delta\mathcal{N}_*)^2}\frac{g_{\rm s}^2}{{\rm Vol}(X_5)}\left(\frac{M_{\rm PL}}{h_{\rm cut}m_{\rm s}}\right)^4 , \tag{B.19}$$

and specifying $g_{\rm s} \sim 10^{-2}$ and ${\rm Vol}(X_5) \simeq \pi^3$ then yields the limit

$$\hat{C} \ll 2.25 \times 10^6 (1-n_s)(-f_{\rm NL}^{\rm eq})^{-1/2} < 5 \times 10^4, \tag{B.20}$$

or equivalently,

$$n \ll 225. \tag{B.21}$$

In deriving the action (5.24) the number of coincident branes was assumed to be large. However we have now found that for the case of branes propagating towards the bulk, the number of such branes is bounded from above. Furthermore, since $f_1 f_2 \simeq$ constant for the AdS_5 throat, the stronger form of the inequality (4.33) may be used. The right hand side of inequality (5.35) would be reduced by a factor of $(\mathcal{N}_{\rm eff}/\Delta\mathcal{N}_*)^2$ by substituting $\Delta\mathcal{N}_* \to \mathcal{N}_{\rm eff}$. This ratio could be as high as $(60/4)^2 \simeq 200$, leading to n being less than 15. In this case the assumption of large n would clearly be inconsistent and the model would be ruled out.

B.1.11. Point 11: Changed "hybrid" to "toy model"

All mentions of the hybrid model have been changed.

Change in list of models on Pg 102:

4. $V(\varphi) = U_0 + \frac{1}{2}m_0^2\varphi^2$. This is a contrived toy model which requires inflation to be terminated by hand. We will set inflation to end when $\varphi \simeq 8$. By taking a value of $U_0 = 5 \times 10^{-10} M_{\rm PL}^4$ a blue spectrum ($n_s > 1$) can then be obtained [104, 120].

Change in description on Pg 129: The fourth model, with potential $V(\varphi) = U_0 + \frac{1}{2}m_0^2\varphi^2$, is a contrived toy model. As described in Section 7.2.1, in order to perform the single field calculation, the end time of inflation must be specified by hand.

Change in caption of Fig 8.12 on Pg 131: Comparison of the source term evolution for the four different models. After horizon crossing the magnitude of the source term is larger for the quadratic and quartic models than for the other two. Towards the end of the numerical calculation there is a marked increase in $|S|$ for three of the models as $\bar{\varepsilon}_H$ increases towards unity. The end time of inflation is specified by hand for the contrived toy model, so this effect is not seen.

B.1.12. Point 12: Initial Conditions

The initial conditions for the second order perturbations are set in Section 7.2.2 on Pg 105. It was suggested that these conditions introduce a spurious homogeneous solution into the final solution for $\delta\varphi_2$ as shown in Fig 8.2. What follows is an analysis of the homogeneous solution and the chosen initial conditions showing that, for the initial conditions we have chosen, the homogeneous solution is zero at all times. This discussion has been added as Appendix A.3.

The homogeneous equation for the second order perturbations is

$$\delta\varphi_2''(\eta, k^i) + 2\mathcal{H}\delta\varphi_2'(\eta, k^i) + \left[k^2 + a^2 V_{,\varphi\varphi} - 24\pi G(\varphi_0')^2\right]\delta\varphi_2(\eta, k^i) = 0\,. \qquad \text{(B.22)}$$

During slow roll, with the slow roll variables ε_H and η_H defined in Chapter 2, this becomes

$$\delta\varphi_2'' + 2\mathcal{H}\delta\varphi_2' + \left[k^2 + 3\mathcal{H}^2(\eta_H + \varepsilon_H)\right]\delta\varphi_2 = 0\,. \qquad \text{(B.23)}$$

If we let $u = a\delta\varphi_2$, this equation can be rewritten as

$$u'' + \left[k^2 + \mathcal{H}^2(3\eta_H - 2\varepsilon_H - 2)\right] u = 0\,. \tag{B.24}$$

When ε_H is small, the conformal time η is given by

$$\eta \simeq -\frac{1}{\mathcal{H}(1-\varepsilon_H)}\,, \tag{B.25}$$

so we can rewrite Eq. (B.24) as

$$u'' + \left[k^2 + \frac{1}{(-\eta)^2}\frac{3\eta_H - 2\varepsilon_H - 2}{(1-\varepsilon_H)^2}\right] u = 0\,. \tag{B.26}$$

If the derivatives are taken in terms of $(-\eta)$ instead of η this is in the form of a Bessel equation with solutions in terms of Hankel functions given by

$$u_{1,2} = \sqrt{-\eta} H_\nu^{(1,2)}(-k\eta)\,, \tag{B.27}$$

where $H_\nu^{(1,2)}$ are the Hankel functions (Bessel functions of the third kind), and ν is given by

$$\nu^2 = \frac{6\varepsilon_H - 12\eta_H + 7}{4(1-2\varepsilon_H)}\,. \tag{B.28}$$

The full solution for u is then

$$u_{\text{full}} = C_1\sqrt{-\eta} H_\nu^{(1)}(-k\eta) + C_2\sqrt{-\eta} H_\nu^{(2)}(-k\eta)\,, \tag{B.29}$$

where $C_1, C_2 \in \mathbb{C}$. When the (real) argument of the Hankel functions goes to $+\infty$ they have the following asymptotic form [1]:

$$H_\nu^{(1)}(z) \to \sqrt{\frac{2}{\pi z}} e^{i(z - \frac{\pi}{2}\nu - \frac{\pi}{4})}\,, \tag{B.30}$$

$$H_\nu^{(2)}(z) \to \sqrt{\frac{2}{\pi z}} e^{-i(z - \frac{\pi}{2}\nu - \frac{\pi}{4})}\,. \tag{B.31}$$

So at early times when $\eta \to -\infty$ and $-k\eta \to +\infty$ we have the following expres-

sions for u:

$$u_i = \sqrt{\frac{2}{\pi k}}\left(C_1 e^{-i(k\eta+\frac{\pi}{2}\nu+\frac{\pi}{4})} + C_2 e^{+i(k\eta+\frac{\pi}{2}\nu+\frac{\pi}{4})}\right) , \tag{B.32}$$

$$u_i' = ik\sqrt{\frac{2}{\pi k}}\left(-C_1 e^{-i(k\eta+\frac{\pi}{2}\nu+\frac{\pi}{4})} + C_2 e^{+i(k\eta+\frac{\pi}{2}\nu+\frac{\pi}{4})}\right) , \tag{B.33}$$

$$\tag{B.34}$$

where we have assumed that ν is slowly varying far in the past, i.e., the derivatives of the slow roll parameters are very small. The initial conditions used in Section 7.2.2 are $\delta\varphi_2 = 0, \delta\varphi_2^\dagger = 0$ at some initial time when the first order perturbations are initialised. If we let η_* denote this initial time then from $u_* = 0$ we have

$$C_1 e^{-i(k\eta+\frac{\pi}{2}\nu+\frac{\pi}{4})} = -C_2 e^{+i(k\eta+\frac{\pi}{2}\nu+\frac{\pi}{4})} . \tag{B.35}$$

We know that $u' = (a\delta\varphi_2)' = \mathcal{H}\delta\varphi_2 + a\mathcal{H}\delta\varphi_2^\dagger$ so setting $\delta\varphi_2 = 0 = \delta\varphi_2^\dagger$ gives

$$C_1 e^{-i(k\eta+\frac{\pi}{2}\nu+\frac{\pi}{4})} = +C_2 e^{+i(k\eta+\frac{\pi}{2}\nu+\frac{\pi}{4})} . \tag{B.36}$$

For these initial conditions then clearly we have

$$C_2 e^{+i(k\eta+\frac{\pi}{2}\nu+\frac{\pi}{4})} = -C_2 e^{+i(k\eta+\frac{\pi}{2}\nu+\frac{\pi}{4})} , \tag{B.37}$$

and so $C_2 = 0 + 0i$ and $C_1 = 0 + 0i$ for these initial conditions.

With this choice of initial conditions for the ordinary differential equation the homogeneous solution is identically zero throughout the evolution. This has also been shown numerically by solving Eq. (B.22) using a Runge-Kutta scheme and the background values for $\mathcal{H}$ and $\varphi + 0$.

The following note has been added to the main text in Section 7.2.2 on Pg 106:

In addition, the perturbations in the far past are supposed to have been purely Gaussian and so at this time the second order perturbation would be zero. With this choice of initial conditions for $\delta\varphi_2$ the homogeneous part of the solution of Eq. (7.13) can be calculated as done in Appendix A.3. The result is that the homogeneous part of the solution is zero for all times.

B.1.13. Point 13: Move some calculations into an appendix

Three large sections of calculations have been moved into the appendix.

All of Section 5.2.2 on Pg 68 has been moved to Appendix A.1.

A part of Section 5.5.2 on Pg 81 has been moved to Appendix A.2.

The calculations of the analytic solutions for $\mathcal{B}$, $\widetilde{\mathcal{C}}$ and $\widetilde{\mathcal{D}}$ have been moved to Appendix A.4.

B.1.14. Point 14: Redo figures with unphysical oscillations

Fig 8.9 has been changed to remove the upper plot which showed the source term before all but the smallest mode had been initialised. The relevant text has also been changed. The new figure is shown in Fig B.1.

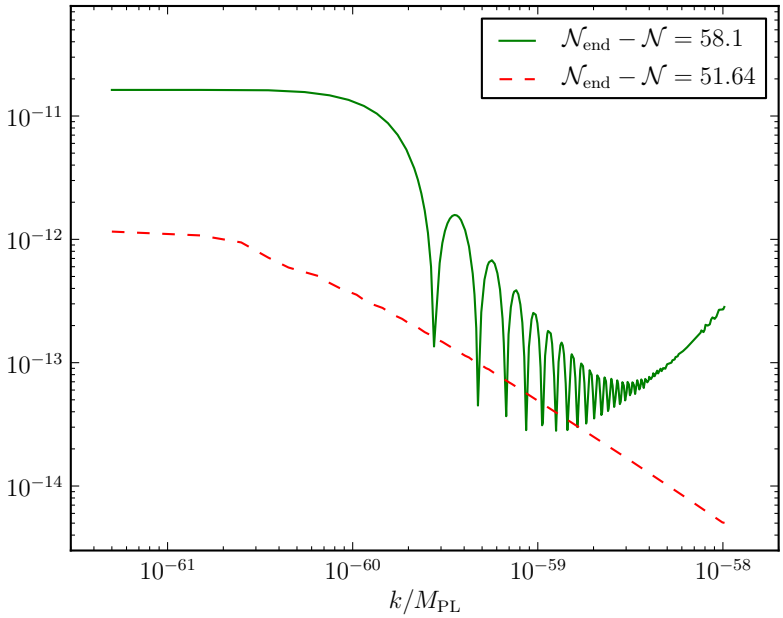

Figure B.1.: The absolute magnitude of the source term for all k values in the range K_1 at two different time steps. The green line shows $|S|$ when all modes have been initialised. The lower red dashed line shows $|S|$ approximately 52 e-foldings before the end of inflation, when all modes have exited the horizon.

Each subfigure in Fig 8.11 has been changed to remove the erroneous sourceterm info before the mode is initialised. The new figures are as shown in Fig B.2.

In the case of the other figures, especially Fig 8.4 on Pg 123 and Fig 8.5 on Pg 124, the small oscillations at early times are not a numerical artifact. The first order perturbations at these times are highly oscillatory as they have not yet been damped sufficiently. (See for example Fig 8.1 on Pg 121.) In convolving the first order perturbations there is

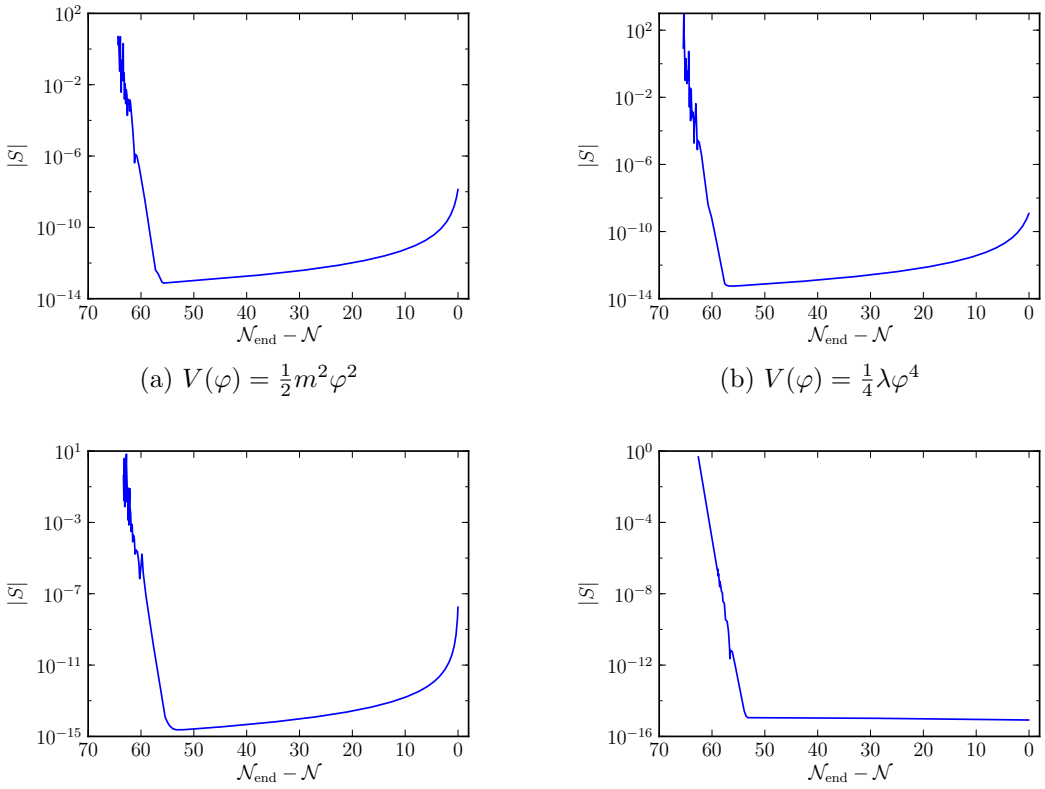

(a) $V(\varphi) = \frac{1}{2}m^2\varphi^2$ (b) $V(\varphi) = \frac{1}{4}\lambda\varphi^4$

(c) $V(\varphi) = \sigma\varphi^{\frac{2}{3}}$ (d) $V(\varphi) = U_0 + \frac{1}{2}m_0^2\varphi^2$

Figure B.2.: Plots of the source term for the four different potentials studied.

no expectation that oscillations in one mode will be matched by those in another. At later times when the first order modes are approximately constant the resulting source term is clearly smoother.

B.1.15. Point 16: Discuss cases where one needs to go beyond slow roll

Added to the Future Directions section (8.3) on Pg 133:

As we have seen the slow roll approximation is very helpful in reducing the equations of motion to a manageable size. However, many interesting models break the assumptions of a slowly rolling field and to investigate these models it is necessary to use the full field equations.

Models in which the field potential is not smooth due to the presence of a feature are particularly interesting examples of single field inflation for which slow roll is broken. As the derivatives of the potential can be large around the feature, these models must necessarily be handled without assumptions about the size of the slow roll parameters. In Ref. [3] a model with a step potential was proposed which takes the form

$$V(\varphi) = \frac{1}{2}m^2\varphi^2\left(1 + c\tanh\left(\frac{\varphi - \varphi_s}{d}\right)\right), \tag{B.38}$$

where φ_s, c and d parametrise the location, height and width of the step feature. A bump model has also been proposed [42], with potential

$$V(\varphi) = \frac{1}{2}m^2\varphi^2\left(1 + c\,\mathrm{sech}\left(\frac{\varphi - \varphi_b}{d}\right)\right), \tag{B.39}$$

where again φ_b, c and d parametrise the feature. At first order these models introduce noticeable differences in the scalar power spectrum. They are also known to be able to produce significant amounts of non-Gaussianity in shapes which are not similar to either the local or equilateral types described in Section 2.6 [41, 42].

It will also be important to go beyond slow roll in the multiple field case. To obtain analytic results, the study of multi-field models has often been restricted to those with either sum or product separable potentials. Even very simple models with two fields such as the double inflation model with the potential given by [184, 197]

$$V(\varphi, \chi) = \frac{1}{2}m_\varphi^2\varphi^2 + \frac{1}{2}m_\chi^2\chi^2, \tag{B.40}$$

can violate slow roll when the fields φ and χ are close to equality. To go some

way towards considering the full range of possible multi-field models with arbitrary inflationary potentials then requires that the full non-slow roll evolution equations are used.

As far as the implementation of the code is concerned, the extension to the non-slow roll single field case is the next step.

B.1.16. Point 17: Elaborate in conclusions and future research directions

Substantial additions have been made to the discussion in Chapter 9. The main changes are listed below.

Changes and additions to discussion on Pg 142:

In Section 4.4, a phenomenological approach was taken to easing the upper bound on the tensor-scalar ratio. By considering a DBI-type action with unspecified field functions, f_i, we showed that the generalised lower and upper bounds can be consistent if the product of f_A and f_B is sufficiently large on observable scales. This provides a guide to the types of models which could evade the inconsistency of the bounds on r. For more general models with a non-canonical action, a bound on r which relates the geometry of the throat, the number of e-foldings of observable inflation, and the derivatives of the action has been derived in Eq. (4.39). This bound, although it does not in general relate to observational quantities can be used when the details of a particular physical model are known.

The discovery of the incompatible bounds on r for DBI inflation has had a noticeable impact on the research community, spurring interest in finding models which evade these bounds. Many such models have been proposed with varying degrees of success. In Section 4.5 these were categorised according to whether they featured single or multiple fields, and single or multiple branes. Some of these models are still constrained by the bounds on r but not to the same extent as the standard DBI scenario. For example the parameter space of the models with wrapped brane configurations is still extremely limited by the observational values from WMAP5 [4]. For other models an analysis in terms of the bounds derived in this thesis has yet to be undertaken. As the observational limits on $f_{\rm NL}^{\rm eq}$ and r continue to improve, an important step in ensuring the validity of DBI based models is to check whether equivalent bounds to those derived here exist, and whether they can be met for any significant proportion of the parameter space.

Added to discussion on Pg 143:

On the other hand, the choice of $r > 10^{-4}$ as the threshold of an observable signal

is very optimistic. If foreground removal techniques and the signal-to-noise ratios of future experiments cannot reach this threshold, and instead reach $r > 10^{-3}$, no number of branes will be able to produce an observable tensor signal when combined with the current limits on the non-Gaussianity. There will then be little possibility of a distinguishing observational signature for these coincident brane models.

Changes and additions to discussion on Pg 144:

The main observable quantity is not however the second order scalar perturbation, but rather the departure from Gaussianity in the CMB temperature map, parametrised by the amplitude of the bispectrum of the perturbations. In Section 6.3 we outlined how $f_{\rm NL}$ could be calculated from the numerically found $\delta\varphi_2$ both for the local type and more generally using the bispectrum of the uniform density curvature perturbation. As the observational limits on $f_{\rm NL}$ are tightened over the course of the remaining WMAP releases and future Planck data, the importance of comparing the predictions for $f_{\rm NL}$ of inflationary models with the observed values will only increase. In this thesis we have not computed $f_{\rm NL}$ for the models we have considered, but this is an important future step that will be undertaken.

...

The initial conditions for the second order perturbations are taken to be $\delta\varphi_2 = 0$ and $\delta\varphi_2^\dagger = 0$ as described in Section 7.2.2. For this choice of initial conditions the homogeneous part of the solution of the second order equation is zero at all times. As the perturbations are supposed to become more Gaussian the further back in time they are considered, in the limit of the far past the second order perturbations should be zero. It remains to be investigated whether the choice of initialisation time is sufficiently far in the past for this assumption to be accurate. At first order it is known that the perturbations are well approximated by the Bunch-Davies vacuum initial conditions even just a few e-foldings before horizon crossing. However, this choice of initialisation time may not be the most appropriate for the second order perturbations. In future work it would be worth considering whether the analytic Green's function solution for $\delta\varphi_2$ at very early times could be integrated until the numerical initialisation time and used as the initial condition for the perturbation.

To test the code, four different, large field, monomial potentials were used. These were the standard quadratic and quartic potentials, a fractional index potential derived from the monodromy string inflation model and a toy model in which inflation is stopped by hand and a blue spectrum is produced. Each potential depends on a single parameter, which was fixed by comparing the resultant scalar curvature power spectrum with the WMAP5 normalisation. The slow roll approximation can be applied to all four potentials. These potentials are not meant to represent an

exhaustive survey of single field slow roll models but are sufficiently different to exhibit different power spectra and second order source terms.

...

The four different potentials have similar amplitudes before horizon crossing but reach different values after horizon crossing. The differences in the slow roll parameters for each potential are compared with the source term values in Appendix A.5. The slow roll parameters do not appear to be directly related to the amplitudes of the source terms, at least in a linear fashion.

Changes and additions to discussion on Pg 146:

Another consideration in the development of a numerical system is the possibility of code re-use. One of our future goals is to develop our code into a numerical toolkit which can be applied to a variety of physical situations. The equations of motion of the inflaton scalar field are similar in form to the governing equations of other important cosmological phenomena. Therefore, it should be possible to adapt the numerical system we have constructed and apply it to other areas of interest. The form of the second order equation and source term are similar to those applicable in the evolution of tensor perturbations and the generation of vorticity in the early universe. The flexibility of the numerical system we have developed will be a positive factor in any attempt to apply our code to these physical systems.

...

When the extension to non slow-roll models is complete, it will be possible to investigate models with a step or other feature in their potential. These models can exhibit large amounts of non-Gaussianity produced around the feature with a shape dependence that is more general than that of the local and equilateral forms.

B.2. Kazuya's Corrections

B.2.1. Point 1: How are constraints on r obtained

Added to discussion in Section 2.4 on Pg 32:

The detection of B-mode polarisation would provide definitive proof of the existence of primordial gravitational modes and much observational effort is being expended in the attempt to achieve such a detection [21, 46, 157, 176, 183, 199]. The observational bound on r from WMAP5 using only the B-mode power spectrum is weak with $r < 4.7$ at the 95% confidence level, when n_s is fixed at the best fit value. Including other polarisation data from the E-mode and TE power spectra reduces this bound to $r < 1.6$, again with n_s fixed. A stronger bound has been ob-

tained with the B-mode power spectrum by the BICEP experiment, giving $r < 0.73$ [46]. The strongest bound to date on the tensor to scalar ratio is given when the temperature power spectrum data is also included in the WMAP analysis. For the pure WMAP5 data without any restriction on n_s but with no spectral running the bound is $r < 0.43$. When BAO and SN data is combined with the WMAP5 data the bound on the tensor to scalar ratio becomes

$$r < 0.20\,, \tag{B.41}$$

at the 95% confidence level.

B.2.2. Point 2: Differences between local and equilateral non-Gaussianity

Added to Section 2.7 on Pg 35:

The main difference between the local and equilateral types of non-Gaussianity are the eras and methods of production. Local non-Gaussianity parametrises non-linear correlations which are local in real space. Non-linear processes taking place outside the horizon are the cause of these correlations. This is Production of this type of non-Gaussianity occurs irrespective of whether the perturbations are Gaussian when they cross the horizon. For single field models the magnitude of $f_{\rm NL}^{\rm loc}$ is proportional to the deviation of the scalar curvature power spectrum from scale invariance and is therefore expected to be small. On the other hand, models with multiple fields can produce a large amount of local non-gaussianity by the evolution of a non-inflaton field outside the horizon and the subsequent transfer of fluctuations in this field into curvature perturbations. A detection of non-negligible $f_{\rm NL}^{\rm loc}$ would therefore be a very strong indication that multiple degrees of freedom are present in the early universe.

In contrast, equilateral type non-Gaussianity is peaked when the momenta of the three modes are very similar and is generated by higher order derivative terms. Both the time and space derivatives become negligible once the modes have left the horizon and therefore any contribution to the bispectrum peaked in the equilateral shape takes place when the modes are inside the horizon. The extra derivative terms required are found generally in non-canonical models which were discussed in Section 2.5. In this case the amplitude of $f_{\rm NL}^{\rm eq}$ is proportional to the inverse of the sound speed squared and can be large.

In the case of single field DBI inflation, discussed in Part I of this thesis, the non-canonical action in Eq. (3.11) contains a non-linear function of $\partial_\mu\varphi$ in the square-root

term. These higher derivative terms are related to the magnitude of the equilateral type through Eq. (2.93). In the relativistic limit in which the sound speed is small, $f_{\rm NL}^{\rm eq}$ can become arbitrarily large. Indeed the current observational limit on $f_{\rm NL}^{\rm eq}$ restricts the degree to which the relativistic limit can be reached and tighter bounds on $f_{\rm NL}^{\rm eq}$ could make such a limit inconsistent.

In summary there are two main types of non-Gaussianity, which are produced in very different fashions[2]. Local non-Gaussianity is produced outside the horizon and is comprised of correlations which are local in real space. Equilateral non-Gaussianity is produced by higher derivative terms when similar modes are inside the horizon. It is generated by models which have non-canonical actions.

B.2.3. Point 3: Physical meaning of $f_{\rm NL}$

Added to discussion in Section 2.6 on Pg 34:

We use the WMAP sign convention for $f_{\rm NL}$ throughout. This is the opposite of the Maldacena convention: $f_{\rm NL}^{\rm WMAP} = -f_{\rm NL}^{\rm Maldacena}$. One consequence of this choice of sign is that positive $f_{\rm NL}$ implies a decrease in temperature in the CMB compared to the Gaussian case. This can be seen by noting that at linear order the temperature anisotropy in the CMB can be related to the curvature perturbation by $\mathcal{R}_{\rm G} \simeq -5\Delta T/T$.

B.2.4. Point 4: State $c_{\rm s} \ll 1$ clearly

Added to discussion on Pg 46: We will assume throughout Part I of this thesis that motion takes place in the relativistic limit in which $c_{\rm s} \ll 1$.

B.2.5. Point 5: Rewrite Section 4.4

See Point 8 above.

B.2.6. Point 6: Initial conditions

See Point 12 above.

[2]Not all non-linear processes fit into these two categories and other types have been proposed including one "orthogonal" to the equilateral type [177].

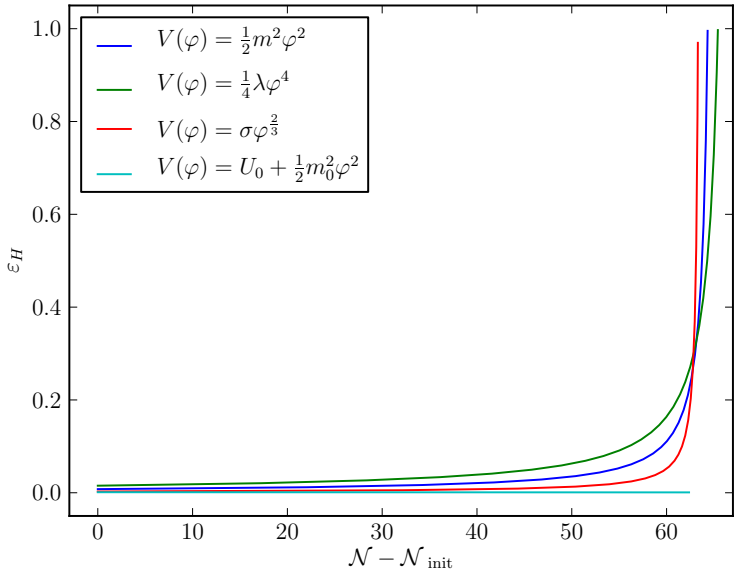

Figure B.3.: The value of ε_H for the four potentials.

B.2.7. Point 7: Plot slowroll parameters and try to explain Fig 8.13

Added as Appendix A.5:

The evolution of the source term for the four potentials has been discussed in Section 8.2.2, with particular emphasis on the evolution after horizon crossing as shown in Figure 8.12. Here the differences apparent at early times, shown in Figure 8.13 are commented on.

At early times the first order perturbations are still very close to the Bunch-Davies initial conditions as outlined in Section 7.2.2. In particular the perturbations are highly oscillatory with phase $\exp(-k\eta)$, where η is the conformal time. When ε_H is small this is given by

$$\eta = -\frac{1}{aH(1-\varepsilon_H)}\,. \tag{B.42}$$

It is therefore instructive to plot the slow roll parameter ε_H for the four potentials at these early times, as has been done in Figures B.3 and B.4. For completeness the other slow roll parameter η_H defined in Eq. (2.27) has been plotted in Figures B.5 and B.6.

Figures B.3 and B.5 show ε_H and η_H for the four different models. Figures B.4 and B.6 show the early stages of the evolution as in Fig 8.13.

As is clear from these figures the change in the slow roll parameters is not easily

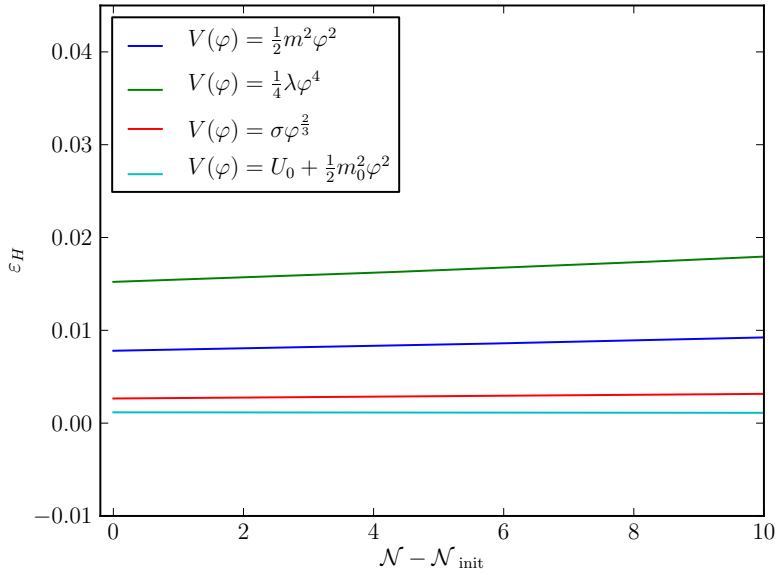

Figure B.4.: The value of ε_H for the four potentials at early times.

related to the differences in the profiles of the four potentials in Figure 8.13. In particular, although ε_H and η_H are quite different for the quadratic and quartic models, the magnitude of S after horizon crossing for these models is very similar.

At the earliest stages of the calculation of S, one or two e-foldings after the initialisation of the first order perturbation, there appear to be small oscillations which affect the models in different ways. The highly oscillatory initial conditions, combined with the small but appreciable differences in ε_H and η_H contribute to this effect. In Figure B.7 the real part of the phase of the initial condition for $\delta\varphi_1$ is plotted just after initialisation for the four potentials. The small differences in phase for each model combined with the sharp cutoff at large and small k values could explain the variations in $|S|$ at early times as seen in Figure 8.13.

B.2.8. Point 8: Check analytic solution

This change has not been completed yet.

B.2.9. Point 9: Add more explanation for why code was developed, and explain how you would calculate f_{NL}

Explanation for code; Added to the discussion of the numerical code in Section 8.4 on Pg 138:

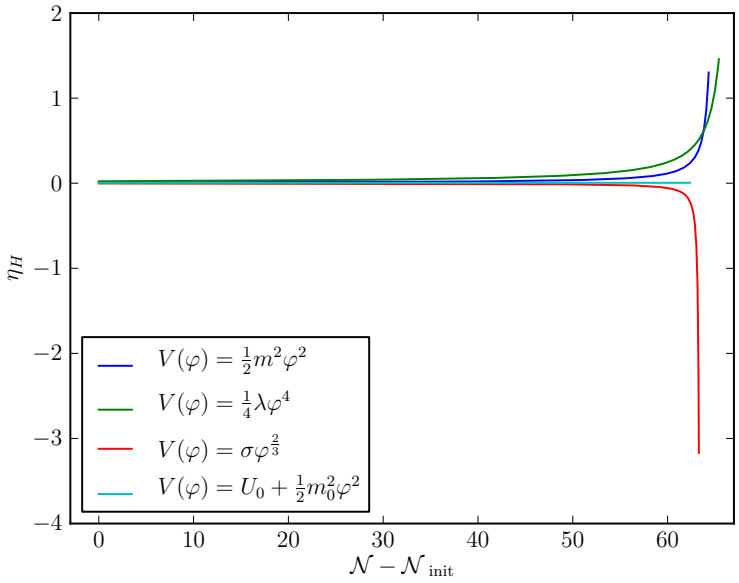

Figure B.5.: The value of η_H for the four potentials.

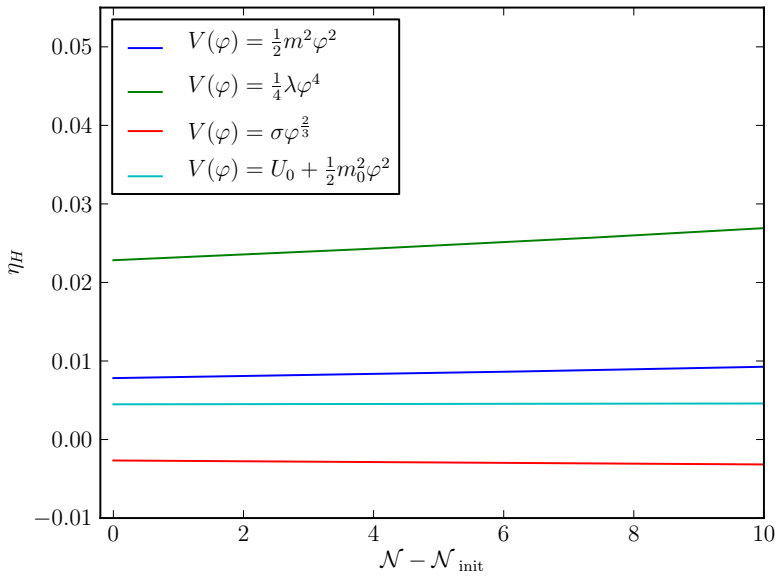

Figure B.6.: The value of η_H for the four potentials at early times.

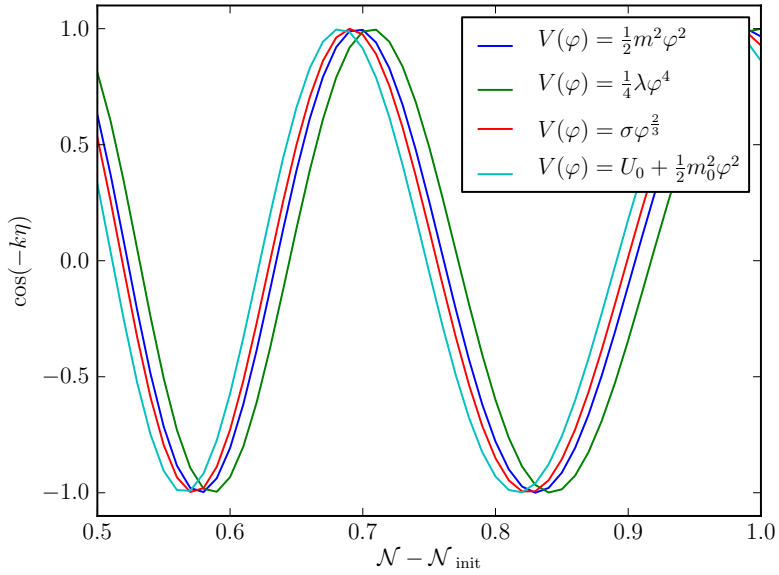

Figure B.7.: The real part of the phase in the Bunch Davies initial conditions for the four different potentials at early times.

Our numerical code evolves the second order perturbation itself and gives an insight into how this field behaves through the full course of the inflationary era. This is in contrast to other approaches which only consider the result for the three point function of the field, or alternatively of the curvature perturbation. The computational system handles perturbations with scales both inside and outside the horizon. Any effects of horizon crossing are visible and no assumptions need to be made about the form of the solution inside the horizon.

The numerical code, when developed with the full equation, will not require any simplifying assumptions about the form of the potential used. This allows models which are not amenable to analytic analysis to be examined. Examples of models which require consideration beyond the slow roll approximation include single field models with a step or other feature in the potential, and multi-field double inflation models where the field values are roughly equal.

The code we have developed is also applicable in other physical circumstances. Beyond scalar perturbations the form of the source term is similar in other interesting cosmological physics. The generation and evolution of non-Gaussian curvature perturbations is, of course, directly related to the behaviour of the second order scalars as has been described in Section 2.6 and Section 6.3. Investigating and classifying non-Gaussian signatures for inflationary models is the main goal of our future work.

The generation of vorticity in a cosmological setting has physical parallels with the equations we have studied. This second order effect arises through the vector perturbations which we have not considered in this thesis. Vorticity in the early universe could also lead to the generation of primordial magnetic fields, an area which is of increasing interest [29, 48]. The wave equations for tensor mode perturbations also exhibit the same form as the scalar equations with a source term at second order. The code we have developed could be modified to examine the behaviour of gravitational waves in the early universe at second order.

Discussion of calculation of $f_{\rm NL}$; Added to Section 6.3 on Pg 93:

To go beyond the local shape of the non-Gaussianity it is necessary to calculate the full bispectrum of the perturbations. In practice the bispectrum of the curvature perturbation on uniform density hypersurfaces, ζ, is used in setting observational limits. At first order this is simply related to the comoving curvature perturbation by $\zeta_1 = -\mathcal{R}_1$. At second order the relationship is more complicated. For large scales outside the horizon, ζ_2 can be related to the field perturbations in real space using [132]

$$\zeta_2(x^i) = -\frac{\mathcal{H}}{\varphi_0'}\delta\varphi_2(x^i) - \left[4 - 3\frac{(\varphi_0')^2 - a^2V_0}{(\varphi_0')^2/2 + a^2V_0}\right]\left(\frac{\mathcal{H}}{\varphi_0'}\right)^2 \delta\varphi_1(x^i)^2 \,. \tag{B.43}$$

In Fourier space this again introduces a convolution integral of the first order perturbations.

The bispectrum of ζ is given by

$$\langle\zeta(\mathbf{k}_1)\zeta(\mathbf{k}_2)\zeta(\mathbf{k}_3)\rangle = (2\pi)^3\delta(\mathbf{k}_1+\mathbf{k}_2+\mathbf{k}_3)B(k_1,k_2,k_3)\,, \tag{B.44}$$

where translation invariance introduces the delta function. The k dependence of the bispectrum is usually separated from an overall amplitude factor and considered as a shape function $F(k_1,k_2,k_3)$. The bispectrum is then of the form [13, 118]

$$\langle\zeta(\mathbf{k}_1)\zeta(\mathbf{k}_2)\zeta(\mathbf{k}_3)\rangle = A(2\pi)^3\delta(\mathbf{k}_1+\mathbf{k}_2+\mathbf{k}_3)F(k_1,k_2,k_3)\,, \tag{B.45}$$

and for a particular shape function F the best estimator for A when the non-Gaussianity is small is given by [13]

$$\hat{A} = \frac{\sum_{\mathbf{k}_i}\zeta(\mathbf{k}_1)\zeta(\mathbf{k}_2)\zeta(\mathbf{k}_3)F(k_1,k_2,k_3)/(\sigma^2_{k_1}\sigma^2_{k_2}\sigma^2_{k_3})}{\sum_{\mathbf{k}_i}F(k_1,k_2,k_3)^2/(\sigma^2_{k_1}\sigma^2_{k_2}\sigma^2_{k_3})}\,, \tag{B.46}$$

where σ_{k_i} is the variance of the mode and the sums run over all the triangles in k

space subject. If $\mathbf{k}_3$ is chosen to be the longest side of the triangle then the triangle inequality enforces

$$k_3 \leq k_1 + k_2 \,. \tag{B.47}$$

Eq. (B.46) provides a blueprint for how to evaluate the bispectrum in terms of a particular given shape. To compare a primordial bispectrum with the observed temperature bispectrum from the CMB it is necessary to construct the spherical harmonics of the bispectrum and use transfer functions to relate the primordial values with the observed values. We have not carried out this procedure in this thesis. However, one of the goals of our future work is to undertake such a comparison of the numerically generated bispectrum with the observed quantity.

As mentioned above, the shape most often used in comparisons with observations is the local shape given by the ansatz in Eq. (2.89). The expression for $F_{\rm local}$ is [13, 105]

$$F_{\rm local}(k_1, k_2, k_3) = 2N f_{\rm NL}^{\rm loc} \left(\frac{1}{k_1^3 k_2^3} + \frac{1}{k_2^3 k_3^3} + \frac{1}{k_1^3 k_3^3} \right) , \tag{B.48}$$

where the spectrum has been taken to be scale invariant and N is a normalisation factor.

This is not the only shape that has been considered and, as we have seen, non-canonical inflationary actions generate a bispectrum which is peaked when the magnitudes of the k modes are approximately equal. The form of F for the equilateral case is [105]

$$F_{\rm eq}(k_1, k_2, k_3) = 6N f_{\rm NL}^{\rm eq} \left\{ -\frac{1}{k_1^3 k_2^3} - \frac{1}{k_2^3 k_3^3} - \frac{1}{k_3^3 k_1^3} - \frac{2}{(k_1 k_2 k_3)^2} + \left[\frac{1}{k_1 k_2^2 k_3^3} + 5\text{perms} \right] \right\} . \tag{B.49}$$

A third form has been proposed which is nearly orthogonal to the other two shapes [177]. These shapes all have the property that they are separable functions of each k_i or can be constructed from these separable functions. This property eases analytic calculations but clearly does not hold for generic shapes. There has been a proposal to define the shape of the bispectrum in terms of a set of basis vector shapes [61, 118]. This would remove the need for only separable shapes to be considered and would allow for a straightforward analysis of the bispectrum from its primordial value up to the observed bispectrum in the CMB.

We have seen that the second order scalar perturbation is not the direct observable quantity of interest. The bispectrum of the curvature perturbations, which

contains a contribution from the second order non-linear part, can be compared with observations either by use of various shape functions or through a full analysis with transfer of the primordial values. A future goal of our work is to compare the bispectrum obtained numerically with that from observations.